ORIGINAL PAPER

Planar π-aromatic C_{3h} $B_6H_3^+$ and π-antiaromatic C_{2h} B_8H_2: boron hydride analogues of D_{3h} $C_3H_3^+$ and D_{2h} C_4H_4

Da-Zhi Li · Hai-Gang Lu · Si-Dian Li

Abstract Based upon extensive density functional theory and wave function theory calculations performed in this work, we predict the existence of the perfectly planar triangle C_{3h} $B_6H_3^+$ (**1**, $^1A'$) and the double-chain stripe C_{2h} B_8H_2 (**9**, ^1A_g) which are the ground states of the systems and the inorganic analogues of cyclopropene cation D_{3h} $C_3H_3^+$ and cyclobutadiene D_{2h} C_4H_4, respectively. Detailed adaptive natural density partitioning (AdNDP) analyses indicate that C_{3h} $B_6H_3^+$ is π plus σ doubly aromatic with two delocalized π-electrons and six delocalized σ-electrons formally conforming to the 4n + 2 aromatic rule, while C_{2h} B_8H_2 is π antiaromatic and σ aromatic with four delocalized π-electrons and ten delocalized σ-electrons. The perfectly planar C_{2h} B_8H_4 (**5**, ^1A_g) also proves to be π antiaromatic analogous to D_{2h} C_4H_4, but it appears to be a local minimum about 50 kJ mol^{-1} less stable than the three dimensional C_s B_8H_4 (**6**, $^1A'$). AdNDP, nucleus independent chemical shifts (NICS) and electron localization function (ELF) analyses indicate that these boron hydride clusters form islands of both σ- and π-aromaticities and are overall aromatic in nature in ELF aromatic criteria.

D.-Z. Li · H.-G. Lu · S.-D. Li (✉)
Institue of Molecular Science, Shanxi University,
Taiyuan 030001, Shanxi, People's Republic of China
e-mail: lisidian@yahoo.com

D.-Z. Li
Department of Chemistry and Chemical Engineering, Binzhou University,
Binzhou 256603, Shandong, People's Republic of China

S.-D. Li
Institute of Materials Science, Xinzhou Teachers' University,
Xinzhou 034000, Shanxi, People's Republic of China

Introduction

As the prototype of electron deficient elements characterized with multicenter bonds in planar networks or cage-like structures, boron has a rich chemistry next only to carbon in the periodic table. Its compounds, especially boron hydrides B_nH_m (n=2-20, n<m), play an essential role in advancing chemical bonding models [1]. Small boron hydride clusters receive consistent attentions in both chemistry and materials science, with typical examples including the reported B_2H_4 [2], BH_3, B_2H_6, B_3H_7, B_4H_{10}, B_5H_9 and B_5H_{11} [3], B_nH^+ (n=1-13) [4], B_2H^+, $B_2H_2^+$, and $B_3H_2^+$ [5], $B_2H_{2n}^{2+}$ dications (n =1-4) [6], and the cage-like B_nH_n neutrals (n=5-13, 16, 19, 22) and their anions $B_nH_n^{-/2-}$ (n=5-13) [7–9]. However, little has been known about the nature of the partially hydrogenated B_nH_m clusters which contain fewer hydrogen atoms than boron atoms (n>m). Limited such examples include the planar $B_7H_2^-$ [10, 11], B_4H_n (n=1-3) [12], and $B_6H_5^+$ [13]. Upon hydrogenation of the convex C_{3v} B_{12} at the six corner positions, Szwacki and coworkers recently predicted the existence of the perfectly planar D_{3h} $B_{12}H_6$ which they called borozene [14]. However, D_{3h} $B_{12}H_6$ was recently proved to be a local minimum lying about 35 kJ mol^{-1} higher than a distorted icosahedral C_2 $B_{12}H_6$ by our group [15]. We have also extended the investigations to $B_{16}H_n$ [16] and $B_{18}H_n$ [17] (n=1-6). To further explore the analogous relationship between boron hydride clusters and their hydrocarbon counterparts, we perform in this work a systematic investigation on the perfectly planar C_{3h} $B_6H_3^+$(**1**) and the double-chain stripe C_{2h} B_8H_2(**9**) which turn out to be the global minima of the systems and the

inorganic analogues of cyclopropene cation D_{3h} $C_3H_3^+$ and cyclobutadiene D_{2h} C_4H_4, respectively. The perfectly planar C_{2h} B_8H_4 (**5**) also appears to be π antiaromatic analogous to D_{2h} C_4H_4, but it proves to be a high-lying local minimum of the system unlikely to be observed in future experiments.

Computational procedures

Structural optimizations and vibrational analyses were performed on the concerned clusters using the hybrid density functional theory (DFT) method of B3LYP [18, 19] with the basis sets of 6-311+G(d,p) implemented in Gaussian03 program [20]. Relative energies for the low-lying isomers were further refined using the coupled cluster method with triple excitations (CCSD(T)) [21–24] at B3LYP geometries (CCSD (T)//B3LYP). Extensive structural searches were performed based upon the low-lying isomers of the bare $B_6^{0/-}$ [25] and $B_8^{0/-}$ [26] by adding terminal hydrogen atoms at corner positions and the low-lying isomers of the boron hydride clusters obtained by using the gradient embedded genetic algorithm (GEGA) method [27, 28]. To elucidate the chemical bonding patterns of these boron hydride clusters, we performed detailed adaptive natural density partitioning (AdNDP) [29–31] analyses on C_{3h} $B_6H_3^+$, C_{2h} B_8H_4, and C_{2h} B_8H_2. To check the π and σ aromaticity/antiaromaticity of the B_nH_m systems, the widely used nucleus independent chemical shifts (NICS) and their perpendicular components along the molecular axes (NICS$_{zz}$) [32, 33] were calculated at points 0.0 Å (NICS(0) and NICS$_{zz}$(0)) and 1.0 Å (NICS$_{zz}$(1)) above the molecular planes using the gauge-independent atomic orbital (GIAO) method [34]. We also employed the electron localization function (ELF) approach [35] of Becke and Edgecombe [36] to analyze the net aromaticity of the concerned clusters. The separated ELF$_\sigma$ and ELF$_\pi$ were constructed using the TopMod [37] software. The one-electron detachment energies of the C_{2h} $B_8H_2^-$ anion were approximated with the time-dependent DFT (TD-DFT) method [38–40] to facilitate its spectroscopic characterizations. Figure 1 shows the four low-lying isomers of $B_6H_3^+$, B_8H_4, B_8H_2 and $B_8H_2^-$ with their relative energies indicated at both B3LYP and CCSD(T)// B3LYP levels. The AdNDP bonding patterns of C_{3h} $B_6H_3^+$ and D_{3h} $C_3H_3^+$ are compared in Fig. 2 and that of C_{2h} B_8H_4, C_{2h} B_8H_2, and D_{4h} C_4H_4 compared in Fig. 3. Figure 4 exhibits the simulated photoelectron spectroscopy (PES) of C_{2h} $B_8H_2^-$.

Fig. 1 Optimized geometries of the four low-lying isomers of (**a**) $B_6H_3^+$ (**1–4**), (**b**) B_8H_4 (**5–8**), (**c**) B_8H_2 (**9–12**), and (**d**) $B_8H_2^-$ (**13–16**), with their relative energies indicated in kJ mol^{-1} at B3LYP and CCSD(T)//B3LYP levels
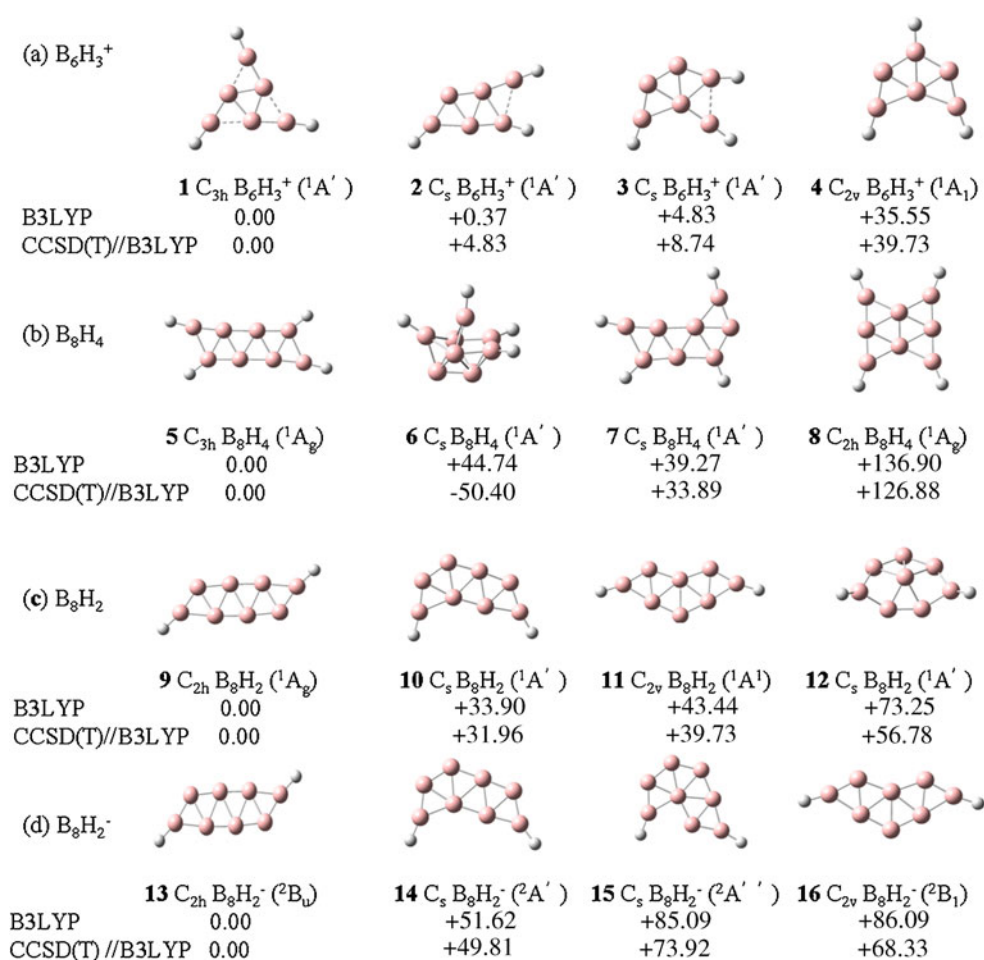
Fig. 2 AdNDP bonding patterns of (a) D_{3h} $C_3H_3^+$ and (b) C_{3h} $B_6H_3^+$ with occupation numbers (ON) indicated
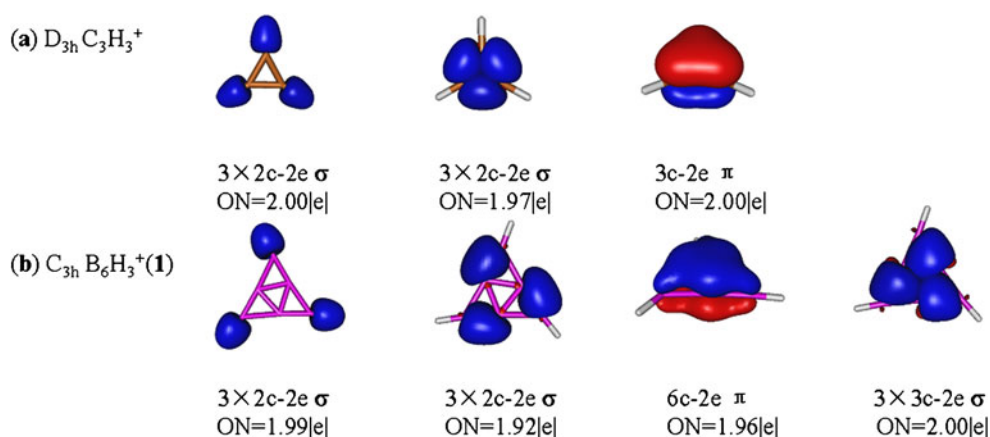

Table 1 tabulates the NICS and $NICS_{zz}$ distributions of C_{3h} $B_6H_3^+$, C_{2h} B_8H_4, and C_{2h} B_8H_2, compared with their hydrocarbon counterparts D_{3h} $C_3H_3^+$ and D_{2h} C_8H_4. Bifurcation values of ELF_σ and ELF_π and their average values (ELF_{av}= $(ELF_\sigma+ELF_\pi)/2$) for $B_6H_3^+(C_{3h},{}^1A')$, $B_8H_4(C_{2h},{}^1A_g)$, and $B_8H_2(C_{2h},{}^1A_g)$ are tabulated in Table 2.

Results and discussion

C_{3h} $B_6H_3^+$ vs D_{3h} $C_3H_3^+$

As shown in Fig. 1a, the planar triangular C_{3h} $B_6H_3^+$ (**1**, ${}^1A'$) is the global minimum of $B_6H_3^+$ which lies 4.83, 8.74 and 39.73 kJ mol^{-1} lower in energy than the elongated C_s $B_6H_3^+$ (**2**,${}^1A'$), C_s $B_6H_3^+$ (**3**,${}^1A'$), and C_{2v} $B_6H_3^+$ (**4**,${}^1A_1$) at CCSD (T)//B3LYP level, respectively. We notice that, as positional isomers, C_{3h} $B_6H_3^+$ (**1**), C_s $B_6H_3^+$ (**2**), and C_s $B_6H_3^+$ (**3**) lie very close in energies (within 8.74 kJ mol^{-1}) and may coexist

in experiments. The triangular B_6 skeleton of C_{3h} $B_6H_3^+$(**1**) is dramatically different from the elongated bare clusters of C_{2h} $B_6^+({}^2B_g)$, C_{2h} $B_6({}^3A_u)$, and D_{2h} $B_6^-({}^2B_{2g})$ [10, 25] upon hydrogenation. A partial hydrogenation of B_6 with three hydrogen atoms leads to the formation of the triangular C_{3h} $B_6H_3^+$(**1**) which contains a equilateral triangle B_3 at the center with the B-B bond length of 1.62 Å. The calculated large HOMO-LUMO gap (4.60 eV) of C_{3h} $B_6H_3^+$ suggests that $B_6H_3^+$ cation is thermodynamically stable, chemically inert, and therefore possible to be characterized in future experiments.

The AdNDP analyses in Fig. 2 provides a clear comparison between C_{3h} $B_6H_3^+$ and cyclopropene cation (D_{3h} $C_3H_3^+$) in bonding patterns. D_{3h} $C_3H_3^+$ possesses three 2c-2e C-H σ-bonds with the occupation numbers of ON=2.00|e|, three 2c-2e C-C σ-bonds with ON=1.97|e|, and one delocalized 3c-2e π-bond with ON=2.00|e|, while its boron hydride counterpart C_{3h} $B_6H_3^+$ (**1**) contains three 2c-2e B-H σ-bonds with ON= 1.99|e|, three 2c-2e B-B σ-bonds with ON=1.92|e|, one
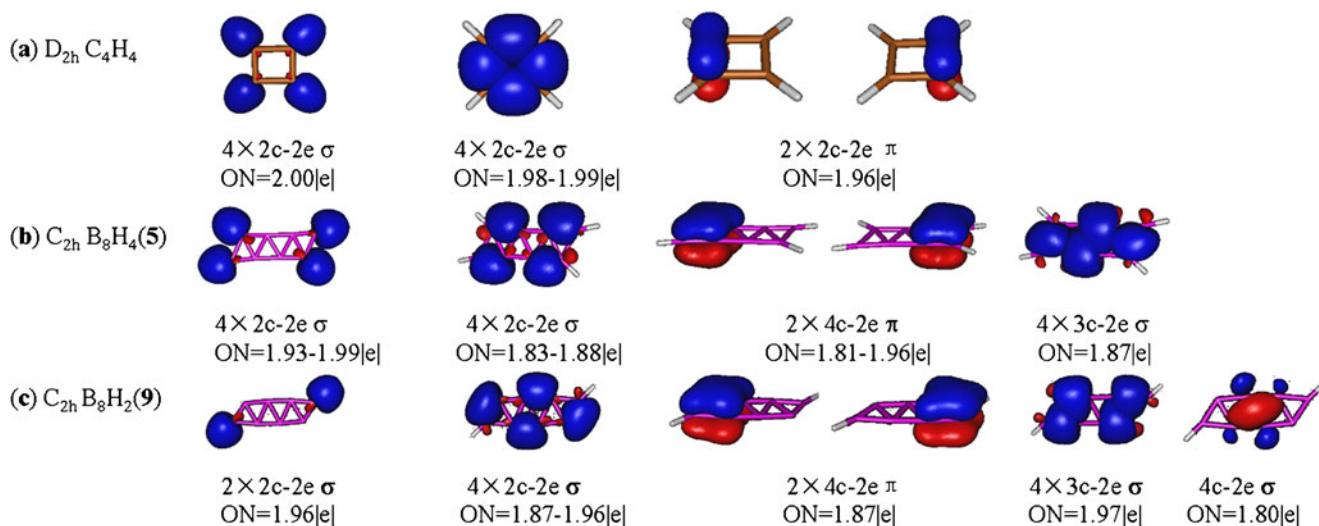

Fig. 3 AdNDP bonding patterns of (a) D_{2h} C_4H_4, (b) C_{2h} B_8H_4, and (c) C_{2h} B_8H_2 with occupation numbers (ON) indicated
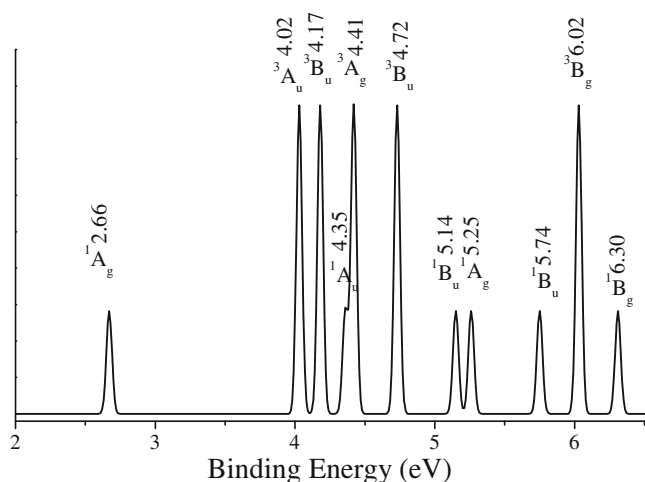
Fig. 4 Simulated PES spectrum of C_{2h} $B_8H_2^-$(**13**) obtained at TD-B3LYP/6-311+G(d, p), with binding energies indicated in eV

delocalized 6c-2e π-bond with ON=1.96|e|, and, in addition, three delocalized 3c-2e σ-bonds with ON=2.00|e|. Obviously, according to the 4n+2 Hückel rule, C_{3h} $B_6H_3^+$(**1**) is formally π plus σ doubly aromatic with two delocalized π-electrons (n=0) and six delocalized σ-electrons (n=1), different from D_{3h} $C_3H_3^+$ which is purely π-aromatic without delocalized σ-electrons. It is the π plus σ double aromaticity that provides extra stability to stabilize C_{3h} $B_6H_3^+$(**1**).

The calculated NICS and NICS$_{zz}$ values of C_{3h} $B_6H_3^+$(**1**) and D_{3h} $C_3H_3^+$ are compared in Table 1. NICS$_{zz}$ has appeared to be a better indicator of π-aromaticity for planar molecules [32, 33]. For C_{3h} $B_6H_3^+$(**1**), the calculated NICS$_{zz}$(0) and

NICS$_{zz}$(1) values of −58.05 and −29.56 ppm at the molecular center (point a) compare well with the corresponding values of −33.07 and −29.23 ppm obtained for D_{3h} $C_3H_3^+$, indicating that C_{3h} $B_6H_3^+$ exhibits strong π-aromaticity analogous to D_{3h} $C_3H_3^+$. The negative NICS(0) (−11.57 ppm) and NICS$_{zz}$(0) (−65.97 ppm) values at points off the molecular centers (point b and equivalent positions) reflect partially the contributions from the three delocalized 3c-2e σ-bonds of C_{3h} $B_6H_3^+$ (see Fig. 2b), indicating the formation of islands of σ-aromaticity in the cation.

B_8H_4 and B_8H_2 vs C_4H_4

The search for the boron hydride analogue of cyclobutadiene (D_{2h} C_4H_4) started from the planar C_{2h} B_8H_4(**5**). As shown in Fig. 1b, C_{2h} B_8H_4 (**5**, ^1A_g) lies 33.89 and 126.88 kJ mol^{-1} lower in energy than the planar C_s B_8H_4(**7**,$^1A'$) and C_{2h} B_8H_4(**8**, ^1A_g) at CCSD(T)//B3LYP, respectively. However, C_{2h} B_8H_4 (**5**) proves to be 50.40 kJ mol^{-1} less stable than the three dimensional C_s B_8H_4(**6**,$^1A'$). Thus, similar to the rectangular cyclobutadiene (D_{2h} C_4H_4) which is a local minima lying higher than its linear global minimum $H_2C=C=C=CH_2$, the elongated planar C_{2h} B_8H_4(**5**) is a high-lying minima less stable than its 3D isomer C_s B_8H_4(**6**).

The goal to find a global minimum boron hydride analogue of D_{2h} C_4H_4 was achieved at C_{2h} B_8H_2(**9**). As clearly indicated in Fig. 1c, the perfectly planar double-chain strip C_{2h} B_8H_2 (**9**,^1A_g) is indeed the ground state of B_8H_2: it lies 31.96, 39.73 and 56.78 kJ mol^{-1} lower than the three low-

Table 1 Calculated nucleus independent chemical shifts (NICS/ppm and NICS$_{zz}$/ppm) of C_{3h} $B_6H_3^+$, C_{2h} B_8H_4 and C_{2h} B_8H_2 at B3LYP/6-311 + g(d,p), compared with the corresponding hydrocarbons at the same theoretical level
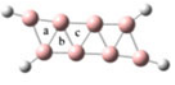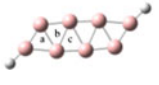
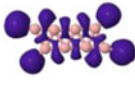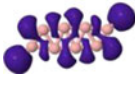|		NICS(0)	NICS$_{zz}$(0)	NICS$_{zz}$(1)
$C_3H_3^+$(D_{3h},$^1A_1'$)	center	-23.65	-33.07	-29.23
$B_6H_3^+$(C_{3h},$^1A'$)	a	-20.92	-58.05	-29.56
	b	-11.57	-65.97	-23.91
C_4H_4(D_{2h},^1A_g)	center	24.73	111.47	55.6
B_8H_4(C_{2h},^1A_g)	center	-21.41	-58.22	-30.06
	a	-16.01	-59.6	-26.62
	b	-17.28	-47.55	-23.51
	c	-23.24	-41.07	-13.65
B_8H_2(C_{2h},^1A_g)	center	-18.25	-53.26	-7.82
	a	-19.79	-46.43	-9.04
	b	-20.54	-29.95	-3.11
	c	-17.54	-47.14	-6.03

Table 2 ELF_σ and ELF_π values and the average bifurcation values ELF_{av} obtained for $B_6H_3^+(C_{3h}, {}^1A')$, $B_8H_4(C_{2h}, {}^1A_g)$ and $B_8H_2(C_{2h}, {}^1A_g)$

molecules	ELF_σ	ELF_π	average
1 $B_6H_3^+(C_{3h}, {}^1A')$	0.87	0.99	0.93
5 $B_8H_4(C_{2h}, {}^1A_g)$	0.84	0.73	0.76
9 $B_8H_2(C_{2h}, {}^1A_g)$	0.82	0.69	0.75

lying isomers of C_s B_8H_2 (**10**,$^1A'$), C_{2v} B_8H_2 (**11**,$^1A_1$), and C_s B_8H_2 (**12**, $^1A'$) at CCSD(T)//B3LYP, respectively. We notice that the elongated B_8 strip in C_{2h} B_8H_2(**9**) is dramatically different from the centered molecular wheels of C_{2v} $B_8^+(^1B_1)$, D_{7h} $B_8(^3A_2')$, and C_{2v} $B_8^-(^2B_1)$ [9, 25]. The antiaromatic π-bonding systems of C_{2h} B_8H_4 and C_{2h} B_8H_2(**9**) detailed below determine the elongated shapes of these clusters. We also notice that the elongated shape of C_{2h} B_8H_2(**9**) is well maintained in its anion $B_8H_2^-$: the slightly relaxed anionic C_{2h} $B_8H_2^-$(**13**,^2B_u) appears to lie 49.81, 68.33 and 73.92 kJ mol^{-1} lower than C_s $B_8H_2^-$ (**14**, $^2A'$), C_s $B_8H_2^-$ (**15**, $^2A''$) and C_{2v} $B_8H_2^-$ (**16**, $^2B_1$) at CCSD(T)// B3LYP, respectively. Both C_{2h} B_8H_2(**9**) and C_{2h} $B_8H_2^-$(**13**) are, in fact, analogous to the previously reported C_{2v} $B_7H_2^-$ [10, 11] in geometry and bonding.

The AdNDP bonding patterns of C_{2h} B_8H_4 (**5**) and C_{2h} B_8H_2(**9**) are depicted in Fig. 3, compared with that of cyclobutadiene (D_{2h} C_4H_4). Several points deserve to be stressed here. First, although both C_{2h} B_8H_4(**5**) and C_{2h} B_8H_2(**9**) possess two 4c-2e π-bonds which look like the two 2c-2e π-bonds of D_{2h} C_4H_4 in orbital shapes, the π-systems of the former two are fundamentally different from the latter in nature, with the two π-bonds of C_{2h} B_8H_4 (**5**) and C_{2h} B_8H_2(**9**) corresponding to two delocalized 4c-2e molecular orbitals (MOs) over the two ends of the molecular sheets while the two π-bonds of D_{2h} C_4H_4 are localized 2c-2e bonds between two carbon atoms along the short edges of the C_4H_4 rectangle. The two delocalized 4c-2e π-bonds in C_{2h} B_8H_4 (**5**) and C_{2h} B_8H_2(**9**) are expected to lead to the formation of islands of π-aromaticity, similar to the situation in the rhombus D_{2h} Li_4 which forms islands of σ-aromaticity [29–31]. Second, D_{2h} C_4H_4 exhibits no delocalized σ-bonds in AdNDP analyses, while both C_{2h} B_8H_4 (**5**) and C_{2h} B_8H_2(**9**) contain four delocalized 3c-2e σ-bonds which are expected to lead to the formation of island of σ-

aromaticity. Finally, C_{2h} B_8H_2(**9**) has an additional delocalized 4c-2e σ-bond with ON=1.80|e| at the molecular center which does not exist in C_{2h} B_8H_4(**5**). Thus, according to the Hückel rule, C_{2h} B_8H_4(**5**) with four delocalized π-electrons and eight delocalized σ-electrons is formally π plus σ doubly antiaromatic in electron counts, while C_{2h} B_8H_2(**9**) with four delocalized π-electrons and ten delocalized σ-electrons is π-antiaromatic and σ-aromatic in nature. It is the delocalized 4c-2e σ-bond at the center that renders σ-aromaticity to C_{2h} B_8H_2(**9**) and makes it the global minimum of the system. Hydrogenation of B_n boron clusters may change the bonding patterns of the B_n cores and even change the aromatic nature of the system by alternating its orbital energy orders [15–17].

As indicated in Table 1, different from cyclobutadiene (D_{2h} C_4H_4) which is globally antiaromatic with positive NICS and $NICS_{zz}$ values, both C_{2h} B_8H_4(**5**) and C_{2h} B_8H_2(**9**) possess reasonably large negative NICS and $NICS_{zz}$ values due to the formation of islands of both π- and σ-aromaticities, with the negative out-of-plane $NICS_{zz}(1)$ mainly indicating the existence of island π-aromaticity and the negative in-plane NICS (0) and $NICS_{zz}(0)$ reflecting partially the contributions from the island σ-aromaticity. The 4n+2 aromatic rule was originally proposed for monocyclic organic molecules. For the boron hydride clusters in triangular motifs studied in this work, it may be applied to specific fragments (B_3 triangles and B_4 rhombus in our case) covered by delocalized mc-2e π- or σ-bonds (m=3 or 4) separately.

ELF analyses

To further strengthen the analyses presented above, detailed ELF analyses [35, 36] were performed in this work to evaluate the net aromaticity of the concerned boron hydride clusters. It has been established by Santos and coworkers that aromatic molecules possess the average bifurcation

values greater than 0.70 on the interval of (0,1) [41]. As clearly indicated in Table 2, with $ELF_\sigma=0.87$, $ELF_\pi=0.99$, and $ELF_{av}=0.93$, the π plus σ doubly aromatic C_{3h} $B_6H_3^+$ is obviously overall aromatic. We notice that, even at the high value of $ELF_\pi=0.99$, the π-basins over the B_6 triangular unit in C_{3h} $B_6H_3^+$ still remain un-split, indicating that the delocalized π-interaction is truly a delocalized 6c-2e bond. For the π plus σ doubly antiaromatic C_{2h} B_8H_4 and the π antiaromatic and σ aromatic C_{2h} B_8H_2, with all the basins beginning to split, $ELF_\sigma=0.84$ and 0.82, $ELF_\pi=0.73$ and 0.69, and $ELF_{av}=0.76$ and 0.75, respectively. Thus, both C_{2h} B_8H_4 and C_{2h} B_8H_2 are overall aromatic in nature in ELF aromatic criteria, consistent with the AdNDP analyses presented above that these clusters all form islands of both σ and π aromaticities (see Fig. 2 and 3) despite their σ- or π-electron counts. In fact, in these electron-deficient boron hydride clusters, all the delocalized π- and σ-electrons occupy bonding MOs, leaving certain portion of the delocalized bonding MOs and all the antibonding MOs empty. Such electron arrangements provide extra electronic delocalization energy to stabilize the systems.

Detachment energies of C_{2h} $B_8H_2^-$

PES measurements in combination with ab initio calculations have proven to be a powerful approach in characterizing various gas-phase clusters [10, 24–27]. As the global minima of the systems, C_{2h} $B_8H_2^{0/-}$ (**9** and **13**) are possible to be produced in experiments by hydrogenation of bare $B_8^{-/0}$ [10, 25] in gas phases. Here, we predict the vertical electron detachment energies (VDEs) of the anionic C_{2h} $B_8H_2^-$(**13**, ^2B_u) and ionization potentials (IP) of neutral C_{2h} B_8H_2(**9**) to facilitate their future characterizations. C_{2h} B_8H_2(**9**) has the calculated high ionization potential of IP=9.12 eV, low electron affinity of AE=2.31 eV, wide HOMO-LUMO gap of 3.15 eV, and the first excitation energy of 1.70 eV at B3LYP/6-311+g(d,p) level. As shown in the simulated PES in Fig. 4, C_{2h} $B_8H_2^-$ anion possesses the first PES peak (X) at VDE=2.66 eV (2.45 eV at CCSD(T)//B3LYP) and a large A-X gap of 1.36 eV between the first peak (X) and the second peak (A). The high-lying excited states of the C_{2h} B_8H_2 neutral are predicted to be closely located in energies which may overlap in PES measurements.

Summary

Given the theoretical predictions presented in Ref. [14–17] and the results obtained in this work, we conclude that small boron hydride clusters C_{3h} $B_6H_3^+$, C_{2h} B_8H_4 (or C_{2h} B_8H_2), D_{3h} $B_{12}H_6$, D_{2h} $B_{16}H_6$, and D_{6h} $B_{18}H_6^{2+}$ which formally conform to the 4n+2 aromatic rule or 4n antiaromatic rule in electron counts form a series of boron hydride analogues of

cyclopropene cation (D_{3h} $C_3H_3^+$), cyclobutadiene (D_{2h} C_4H_4), benzene (D_{2h} C_6H_6), naphthalene (D_{2h} $C_{10}H_8$), and annulene (D_{5h} $C_{10}H_{10}$), respectively. Detailed AdNDP, NICS and ELF analyses indicate that these partially hydrogenated boron hydride clusters B_nH_m (n > m) differ from their hydrocarbon counterparts in the formation of islands of both σ- and π-aromaticity which feature the bonding patterns of the planar or quasi-planar B_n networks and render net aromaticity to the systems in ELF criteria. Partially hydrogenated planar or quasi-planar boron hydride clusters B_nH_m with suitable n/m ratios are expected to serve as stable ligands to transition metals to form a wide range of sandwich complexes.

References

1. Cotton FA, Wilkinson G, Murrillo CA, Bochmann M (1999) Advanced Inorganic Chemistry, 6th edn. Wiley, New York
2. Vincent MA, Schaefer HF (1981) J Am Chem Soc 103:5677–5680
3. Tian SX (2005) J Phys Chem A 109:5471–5480
4. Ricca A, Bauschlicher CW (1997) J Chem Phys 106:2317–2322
5. Curtiss LA, Pople JA (1989) J Chem Phys 91:4809–4812
6. Dias JF, Rasul G, Seidl PR, Surya Prakash GK, Olah GA (2003) J Phys Chem A 107:7981–7984
7. McKee ML, Wang ZX, Schleyer PvR (2000) J Am Chem Soc 122:4781–4793
8. Schleyer PvR, Subramanian G, Dransfeld A (1996) J Am Chem Soc 118:9988–9989
9. Goursot A, Pénigault E, Chermette H, Fripiat JG (1986) Can J Chem 64:1752–1757
10. Alexandrova AN, Boldyrev AI, Zhai HJ, Wang LS (2006) Coord Chem Rev 250:2811–2866
11. Alexandrova AN, Koyle E, Boldyrev AI (2006) J Mol Model 12:569–576
12. Boyukata M, Ozdogan C, Güvenç ZB (2007) J Mol Struct (THEOCHEM) 805:91–101
13. Yu HL, Sang RL, Wu YY (2009) J Phys Chem A 113:3382–3386
14. Szwacki NG, Weber V, Tymczak CJ (2009) J Nanoscale Res Lett 4:1085–1089
15. Bai H, Li SD (2011) J Clust Sci 22:525–535
16. Chen Q, Li SD (2011) J Clust Sci 22:513–523
17. Chen Q, Bai H, Guo JC, Miao CQ, Li SD (2011) Phys Chem. Chem Phys. doi:10.1039/C1CP21927H
18. Becke AD (1993) J Chem Phys 98:5648–5652
19. Lee C, Yang W, Parr RG (1988) J Phys Rev B 37:785–790
20. Frisch MJ, Trucks GM, Schlegel HB, Scuseria GE, Robb MA, Cheeseman JR, Montgomery JA, Vreven T, Kudin KN, BurantJC, Millam JM, Iyengar SS, Tomasi J, Barone V, Mennucci B, Cossi M, Scalmani G, Rega N, Petersson GA, Nakatsuji H, Kitao O, Nakai H, Klene M, Li X, Knox JE, Hratchian HP, Cross JB, Adamo C, Jaramillo J, Gomperts R, Stratmann RE, Yazyev O, Austin AJ, Cammi R, Pomelli C, Ochterski JW, Ayala PY, Morokuma K, Voth GA, Salvador P, Dannenberg JJ, Zakrzewski VG, Dapprich S, Daniels AD, Strain MC, Farkas O, Malick DK, Rabuck AD, Raghavachari K, Foresman JB, Ortiz JV, Cui Q, Baboul AG, Clifford S, Cioslowski J, Stefanov BB, Liu A, Liashenko A, Piskorz P, Komaromi I, Martin RL, Fox DJ, Keith T, Al-Laham MA, Peng CY, Nanayakkara A, Challacombe M, Gill PMW, Johnson BG, Chen W, Wang MW, Gonzales C, Pople JA (2003) Gaussian 03, Revision A.1. Gaussian Inc, Pittsburgh, PA

21. Pople JA, Head-Gordon M, Raghavachari K (1987) J Chem Phys 87:5968–5975
22. Scuseria GE, Schaefer HF III (1989) J Chem Phys 90:3700–3703
23. Scuseria GE, Janssen CL, Schaefer HF III (1988) J Chem Phys 89:7382–7388
24. Cizek J (1969) Adv Chem Phys 14:35–89
25. Alexandrova AN, Boldyrev AI, Zhai HJ, Wang LS, Steiner E, Fowler PW (2003) J Phys Chem A 107:1359–1369
26. Zhai HJ, Alexandrova AN, Birch KA, Boldyrev AI, Wang LS (2003) Angew Chem Int Edn 42:6004–6008
27. Alexandrova AN, Boldyrev AI, Fu YJ, Wang XB, Wang LS (2004) J Chem Phys 121:5709–5719
28. Alexandrova AN, Boldyrev AI (2005) J Chem Theor Comput 1:566–560
29. Zubarev DY, Boldyrev AI (2008) Phys Chem Chem Phys 10:5207–5217
30. Zubarev DY, Boldyrev AI (2008) J Org Chem 73:9251–9258
31. Zubarev DY, Boldyrev AI (2009) J Phys Chem A 113:866–868
32. Schleyer PvR, Maerker C, Dransfeld A, Jiao H, van Eikema Hommes NJR (1996) J Am Chem Soc 118:6317–6318
33. Fallah-Bagher-Shaidaei H, Wannere CS, Corminboeuf C, Puchta R, Schleyer PvR (2006) Org Lett 8:863–866
34. Wolinski K, Hinton JF, Pulay P (1990) J Am Chem Soc 112:8251–8260
35. Silvi B, Savin A (1994) Nature 371:683–686
36. Becke A, Edgecombe K (1990) J Chem Phys 92:5397–5430
37. Noury S, Krokidis X, Fuster F, Silvi B (1997) TopMoD Package, Universite Pierre et Marie Curie, France
38. Casida ME, Jamorski C, Casida KC, Salahub DR (1998) J Chem Phys 108:4439–4450
39. Stratmann RE, Scuseria GE, Frisch MJ (1998) J Chem Phys 109:8218–8224
40. Bauernschmitt R, Ahlrichs R (1996) Chem Phys Lett 256:454–464
41. Santos JC, Andres J, Aizman A, Fuentealba P (2005) J Chem Theor Comput 1:83–86